Stability of a Block-Copolymer Lamella in a Strong Electric Field

M. W. Matsen

Department of Physics, University of Reading, Whiteknights, Reading, RG6 6AF, United Kingdom

(Received 27 June 2005; published 16 December 2005)

Using self-consistent field theory, we examine the stability of a lamellar layer of diblock copolymer subject to strong orthogonal electric fields. Two competing instabilities are identified; one is a peristaltic mode that leads to perpendicular lamellae, and the other is an undulatory mode that results in the formation of an undesirable grain boundary. The former kinetic pathway is favored when the central domain is relatively thin and composed of the low-dielectric material.

DOI: 10.1103/PhysRevLett.95.258302 PACS numbers: 83.80.Uv, 64.70.Nd, 81.16.Rf

AB diblock copolymers are long-chain molecules of N segments, where the first fN are of type A and the remaining $(1-f)N$ are of type B. The natural tendency (measured by the Flory-Huggins χ parameter) for unlike segments to segregate results in the formation of periodically ordered morphologies [1]. Researchers are now exploiting this self-assembly to fabricate nanoscale structures [2], either directly from the block-copolymer material [3], as scaffolds for arranging other molecules or nanoparticles [4,5], or as templates for nanolithography [6]. Possible applications and devices include high-density information storage [6], waveguides [7], nanoporous membranes [3,4], and nanowires [5,8]. Although the self-assembly process is exceptionally efficient, it does not always produce the desired pattern; the common examples being that lamellar and cylindrical domains tend to orient parallel to the substrate, as opposed to perpendicular where they exhibit a more useful lateral structure. Researchers [9] have coated the substrates to negate the surface interactions that cause this, but the resulting structures are generally populated by numerous defects. One strategy for overcoming this problem is to orient the domains using strong electric fields that couple to the contrast between the dielectric constants, κ_A and κ_B, of the A and B components [10,11].

Here we combine self-consistent field theory (SCFT) [12] with an exact treatment for linear dielectric materials to produce a rigorous method of investigating the free-energy landscape, $F[\Phi]$, of structured polymeric systems (e.g., polymer brushes, polymer blends, and block copolymers) with respect to their composition profile, $\Phi(\mathbf{r})$. The method is demonstrated on a parallel lamellar layer of volume $\mathcal{V}$ containing n diblock copolymers sandwiched between two parallel conductors. Two competing instabilities are identified (depicted in Fig. 1), and the resulting kinetic pathways towards perpendicular lamellae are investigated. There have been two related calculations for multilamellar films, but less sophisticated; Ref. [13] examined the undulatory instability, while Ref. [14] tested the global stability of parallel lamellae.

The principle approximation in SCFT is to represent the molecular interactions by mean (i.e., nonfluctuating) fields, $w_A(\mathbf{r}) \equiv u(\mathbf{r}) + w(\mathbf{r})$ and $w_B(\mathbf{r}) \equiv u(\mathbf{r}) - w(\mathbf{r})$, which act on A and B segments, respectively. The fields are adjusted so that the dimensionless A- and B-segment concentrations satisfy the incompressibility condition, $\phi_A(\mathbf{r}) + \phi_B(\mathbf{r}) = 1$, and the specified composition profile, $\Phi(\mathbf{r}) \equiv \phi_A(\mathbf{r}) - \phi_B(\mathbf{r})$. Once this is achieved, the free energy is given by

$$\frac{F[\Phi]}{nk_BT} = -\ln\mathcal{Q} - \sum_{\mathbf{k}\neq 0}\left(\frac{\chi N}{4}\Phi_{\mathbf{k}}\Phi_{-\mathbf{k}} + w_{\mathbf{k}}\Phi_{-\mathbf{k}}\right) - \mathcal{E},$$

where $\mathcal{Q}$ is the partition function of a single molecule in the fields [12] and $\mathcal{E}$ is the electric-field energy per molecule in units of k_BT [10]. Note that spatially varying quantities are expanded in Fourier series, such as

$$\Phi(\mathbf{r}) = \sum_{\mathbf{k}}\Phi_{\mathbf{k}}\exp(i\mathbf{k}\cdot\mathbf{r}).$$

The sum extends over the wave vectors,

$$\mathbf{k} = (2\pi n_x/D_\perp)\hat{\mathbf{e}}_x + (\pi n_z/D_\parallel)\hat{\mathbf{e}}_z,$$

where n_x and n_z are integers. In practice, the large wave vectors are truncated based on an acceptable error tolerance. The surfaces at $z = 0$ and $z = D_\parallel$ are treated as reflecting boundaries enforced by choosing real coefficients with $\Phi_{\mathbf{k}} = \Phi_{-\mathbf{k}} = \Phi_{\bar{\mathbf{k}}} = \Phi_{-\bar{\mathbf{k}}}$, where $\bar{\mathbf{k}}$ denotes the complimentary wave vector obtained by reversing the

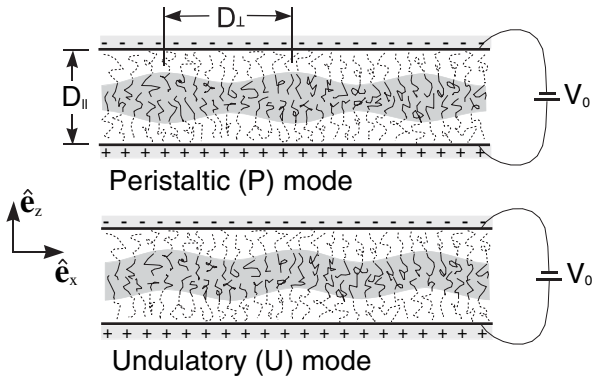

FIG. 1. The two competing instabilities of a block-copolymer lamella subjected to an external electric field, $E_0 = V_0/D_\parallel$. Note that both these modes are uniform in the $\hat{\mathbf{e}}_y$ direction.

sign of n_z. For simplicity, we ignore the surface affinity for B segments responsible for the initial parallel alignment, because it does not significantly affect our results until the later stages of the kinetic pathway where the A-rich domain begins to contact the conducting plates.

The electric field between the plates is expressed as $\mathbf{E} = -E_0\nabla\upsilon$, where the scaled potential satisfies the boundary conditions $\upsilon = 0$ at $z = 0$ and $\upsilon = -D_\parallel$ at $z = D_\parallel$. This is achieved by expanding as

$$\upsilon(\mathbf{r}) = -z - i\sum_{\mathbf{k}\neq 0} \upsilon_{\mathbf{k}} \exp(i\mathbf{k}\cdot\mathbf{r}),$$

with real Fourier coefficients that satisfy $\upsilon_{\mathbf{k}} = -\upsilon_{-\mathbf{k}} = \upsilon_{\bar{\mathbf{k}}} = -\upsilon_{-\bar{\mathbf{k}}}$. The potential is evaluated using the Maxwell equation, $\nabla\cdot(\kappa\mathbf{E}) = 0$, where $\kappa(\mathbf{r}) \equiv \kappa_A\phi_A(\mathbf{r}) + \kappa_B\phi_B(\mathbf{r})$. When expressed in Fourier coefficients, the equation becomes

$$k_z\kappa_{\mathbf{k}} = \sum_{\mathbf{g}} \mathbf{k}\cdot\mathbf{g}\kappa_{\mathbf{k}-\mathbf{g}}\upsilon_{\mathbf{g}}.$$

Once $\upsilon(\mathbf{r})$ is known, the electric-field energy is given by

$$\mathcal{E} \equiv \frac{\epsilon_0 E_0^2}{2nk_BT}\int \kappa(\nabla\upsilon)^2 d\mathbf{r} = \mathcal{E}_D\left[1 + \kappa_\Delta\sum_{\mathbf{k}} k_z\Phi_{\mathbf{k}}\upsilon_{-\mathbf{k}}\right],$$

where

$$\mathcal{E}_D = \epsilon_0\bar{\kappa}E_0^2\mathcal{V}/2nk_BT$$

represents the field energy of a disordered melt and

$$\kappa_\Delta = (\kappa_A - \kappa_B)/2\bar{\kappa}, \qquad \bar{\kappa} \equiv f\kappa_A + (1-f)\kappa_B$$

specify the dielectric contrast and the average dielectric constant, respectively.

Testing stability and following kinetic pathways requires us to evaluate the change in free energy,

$$\frac{\delta F}{nk_BT} \approx \sum_{\mathbf{k}}\Omega_{\mathbf{k}}\delta\Phi_{-\mathbf{k}} + \frac{1}{2}\sum_{\mathbf{k},\mathbf{g}}[\mathbf{C}^{-1}_{\mathrm{RPA}}]_{\mathbf{k},\mathbf{g}}\delta\Phi_{-\mathbf{k}}\delta\Phi_{\mathbf{g}},$$

produced by a small variation, $\delta\Phi(\mathbf{r})$, in the composition profile [15,16]. The coefficients of the first-order term are

$$\Omega_{\mathbf{k}} = -w_{\mathbf{k}} - \frac{\chi N}{2}\Phi_{\mathbf{k}} - \frac{\partial\mathcal{E}}{\partial\Phi_{-\mathbf{k}}},$$

from which the self-consistent field condition for stable or metastable morphologies is given by $\Omega_{\mathbf{k}} = 0$. The second-order coefficients take the form

$$[\mathbf{C}^{-1}_{\mathrm{RPA}}]_{\mathbf{k},\mathbf{g}} = [\tilde{\mathbf{C}}^{-1}]_{\mathbf{k},\mathbf{g}} - \frac{\chi N}{2}\delta_{\mathbf{k},\mathbf{g}} - \frac{\partial^2\mathcal{E}}{\partial\Phi_{-\mathbf{k}}\partial\Phi_{\mathbf{g}}},$$

where the calculation of $\tilde{\mathbf{C}}^{-1}$, which accounts for variations in $-\ln\mathcal{Q}$, is described in Ref. [15]. The morphology is stable or metastable only if all the eigenvalues λ_α of $\mathbf{C}^{-1}_{\mathrm{RPA}}$ are positive at all wavelengths, $D_\perp$. Once an eigenvalue becomes negative, the morphology will evolve in the direction of the associated eigenvector towards a new free-energy minimum.

We now demonstrate our technique by applying it to the simple case depicted in Fig. 1 of a single lamella sandwiched between two conducting plates. Assuming the lamella orders prior to the addition of the upper conductor, we set the film thickness, $D_\parallel$, equal to the bulk lamellar period, D_b [17]. The dielectric contrast is fixed at $|\kappa_\Delta| = 0.4$, characteristic of polystyrene-polymethylmethacrylate (PS-PMMA) diblock copolymers [8,18,19]. We do, however, consider both signs of κ_Δ, where the central A-rich domain is either the high- or low-dielectric material (i.e., PMMA or PS, respectively). For the moment, we examine symmetric diblocks ($f = 0.5$) at a fixed intermediate segregation ($\chi N = 15$), but we will adjust these parameters latter.

The two dominant (i.e., smallest) eigenvalues of $\mathbf{C}^{-1}_{\mathrm{RPA}}$ correspond to peristaltic and undulatory modes, which we denote as P_+ and U_+ for $\kappa_\Delta > 0$ and as P_- and U_- for $\kappa_\Delta < 0$. Figure 2 plots the eigenvalues λ_α of these modes as a function of lateral periodicity, $D_\perp$, at an electric-field strength $\mathcal{E}_D = 3.5$, where both modes are unstable. At the composition of $f = 0.5$, the P instability is completely unaffected by the sign of κ_Δ, whereas the U instability is enhanced by placing the high-dielectric material at the center of the film.

To find where the P and U instabilities lead, we traverse the free-energy landscape along the path of steepest decent [15]. This is done using our expression for δF and taking small steps of $\delta s = 0.01$, defined by the Euclidean metric,

$$\delta s^2 = \frac{1}{\mathcal{V}}\int \delta\Phi^2(\mathbf{r})d\mathbf{r} = \sum_{\mathbf{k}}\delta\Phi_{\mathbf{k}}\delta\Phi_{-\mathbf{k}}.$$

After each step, Ω and $\mathbf{C}^{-1}_{\mathrm{RPA}}$ are reevaluated, and the process continues until a new free-energy minimum is reached where $\Omega_{\mathbf{k}} = 0$. During this, $D_\perp$ is held fixed because we assume the morphology evolves too quickly for the total number of unit cells to change [15].

Figure 3 shows the reduction in free energy as the P_+ mode grows at the preferred lateral periodicity, $D^*_\perp = 0.976D_b$, indicated by the solid dot in Fig. 2. The insets show a single period of the morphology at several points along the kinetic pathway, illustrating the break-up of the lamella into cylindrical domains (oriented in the y direction) that then transform into perpendicular lamellae. Figure 4(a) shows the alternative pathway originating from the U_- mode at $D^*_\perp = 1.103D_b$. This time the reduction in free energy is more gradual, and the film finishes with two thin perpendicular lamellar phases separated by a metastable grain boundary located down the middle at $z = D_\parallel/2$. The grain boundary can be removed by turning up the electric field, as demonstrated in Fig. 4(b). With the increased field, the free energy decreases as the grain boundary shifts towards one of the conducting plates. However, the decrease is incredibly gradual until the very end where the grain boundary begins to contact the conducting plate.

Assuming the goal is to create perpendicular lamellae, the more direct pathway of the P mode is clearly the better

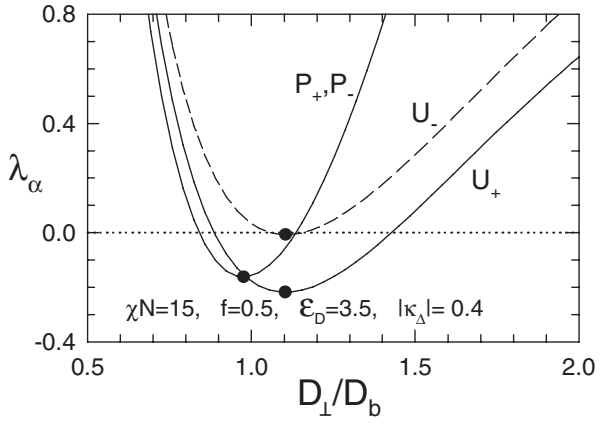

FIG. 2. Dominant eigenvalues of $\mathbf{C}_{\mathrm{RPA}}^{-1}$ (corresponding to the P and U modes in Fig. 1) plotted as a function of lateral periodicity, $D_\perp$, for a field strength of $\mathcal{E}_D = 3.5$. The subscripts, $\pm$, denote calculations at $\kappa_\Delta = \pm 0.4$, respectively.

route. The P mode also has a couple other advantages over the U mode on account of the location and narrowness of its minimum in Fig. 2. First of all, its perpendicular lamellae will be more stable and thus less prone to defects, because $D_\perp^*$ is much better matched to the natural lamellar spacing, D_b [17]. Second of all, the narrower minimum of the P mode should reduce the random variation in the thicknesses of individual lamellae to produce a more regular periodicity.

To ensure that the system chooses this preferred path, we look for conditions where P is the only unstable mode. Figure 5 shows the eigenvalues, λ_α^*, minimized with respect to $D_\perp$, as the field strength is increased. The P_+ and P_- modes both become unstable at $\mathcal{E}_D^* = 3.166$, whereas the U_+ and U_- modes become unstable at the distinct values, 2.892 and 3.478, respectively. Thus, the desired conditions are met by preparing the film with the low-dielectric material at the center (i.e., $\kappa_\Delta < 0$) and selecting $3.166 < \mathcal{E}_D < 3.478$.

Targeting this narrow range requires careful tuning of the electric field, since $\mathcal{E}_D \propto E_0^2$. Fortunately, the situation

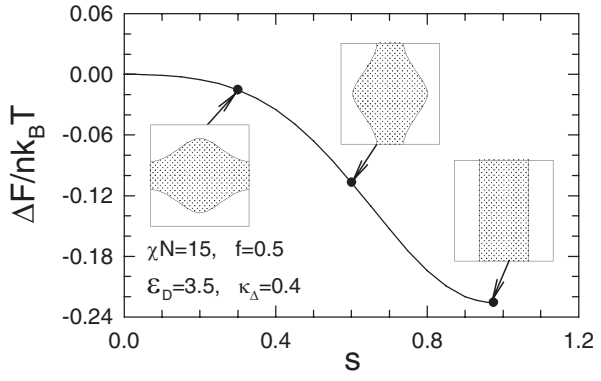

FIG. 3. Change in free energy ΔF as the unstable peristaltic (P_+) mode grows at the preferred lateral periodicity, $D_\perp^*$, marked by a solid dot in Fig. 2. The insets show the evolution of one period at several points along the kinetic pathway.

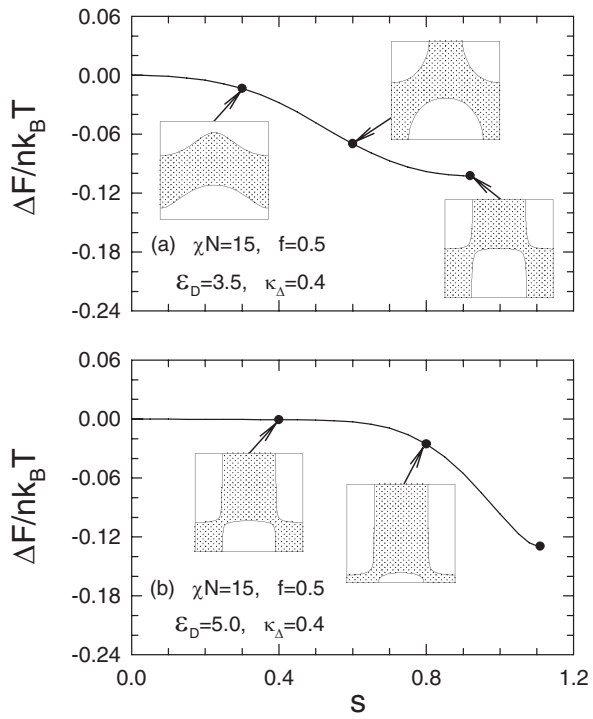

FIG. 4. (a) Analogous plot to that of Fig. 3, but starting from the unstable undulatory (U_+) mode. (b) Continuation of the kinetic pathway once the electric field is amplified.

can be improved by adjusting the diblock composition. As illustrated in Fig. 6(a), the interval increases to $1.796 < \mathcal{E}_D < 3.221$ for $f = 0.4$ and $\kappa_\Delta = -0.4$. The reduction in the lower bound will also help experimentalists avoid dielectric breakdown. If necessary, the critical fields can be further reduced by lowering the level of segregation, χN, as demonstrated by Fig. 6(b).

Experiments have yet to investigate single layers, but Ref. [18] has examined multilamellar stacks of $f = 0.5$ PS-PMMA diblocks at a segregation of $\chi N \approx 26$. They are able to induce orientation with $E_0 \approx 40$ V/μm, which corresponds to a $\mathcal{E}_D \approx 0.6$, well below the critical $\mathcal{E}_D^*$

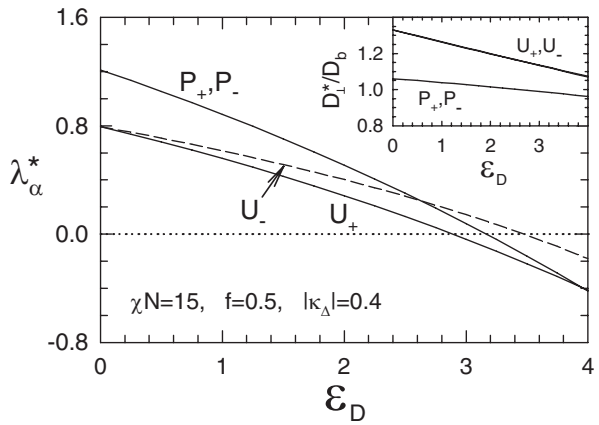

FIG. 5. Eigenvalues of $\mathbf{C}_{\mathrm{RPA}}^{-1}$ evaluated at the preferred lateral periodicity, $D_\perp^*$ (shown in the inset), and plotted as a function of the field strength $\mathcal{E}_D$.

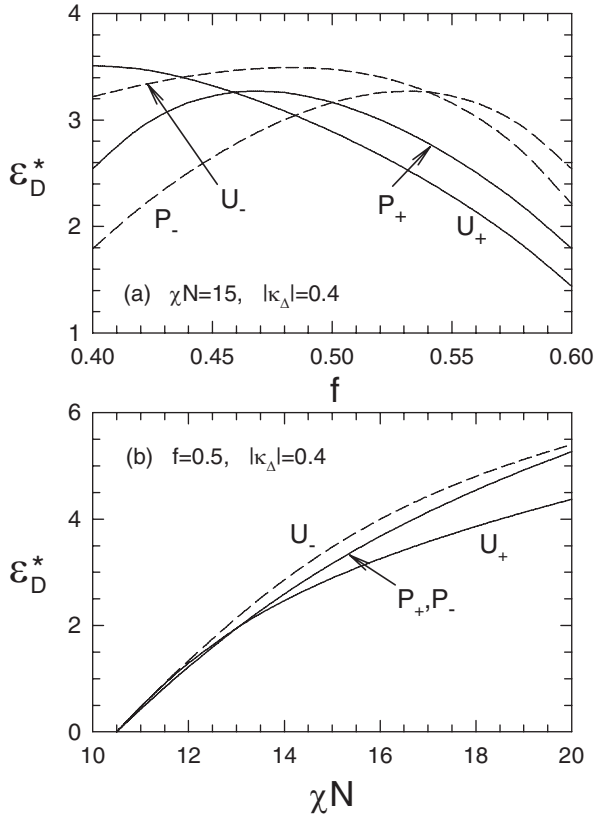

FIG. 6. Critical field strength $\mathcal{E}_D^*$ plotted as a function of (a) diblock composition f and (b) segregation χN.

indicated by Fig. 6(b). Multilayer stacks do have additional lower-energy U modes, where neighboring lamellae undulate in unison [13], but it is likely the presence of defects that facilitate orientation at such low $\mathcal{E}_D$. Indeed, the defect-free lamellae that form next to the walls (when the surface affinity is not too weak) are unaffected by their electric fields.

Although our theory can handle multilamellar stacks with defects, it is unlikely that the kinetic pathways would lead to well-ordered morphologies. Furthermore, there are clear advantages of studying model systems free of defects, but dielectric breakdown may then prevent experiments from accessing $\mathcal{E}_D^*$. Although reductions in λ_α could still be investigated by observing capillary-wave fluctuations [20], there are also potential ways of lowering $\mathcal{E}_D^*$. For instance, the segregation could be reduced with a neutral solvent that could be evaporated off once the domains were reoriented. Alternatively, small amounts of homopolymer could be added to relieve the packing frustration [12] that tends to prevent modulations in the domain thickness. Tsori *et al.* [21] suggest that a small concentration of mobile ions may aid the process, which could be modeled with our improved theory by using the generalized Maxwell equation, $\nabla \cdot (\boldsymbol{\kappa}\mathbf{E}) = \rho_f/\epsilon_0$, where ρ_f is the density of the *free* charges.

Not only is our SCFT treatment of electric-field effects sufficiently versatile to handle all the variations suggested above, it is also the most rigorous theory to date. The polymers are represented as Gaussian chains and treated as linear dielectrics, while the statistical mechanics is performed in the mean-field approximation. Beyond that, there are no further approximations and numerical uncertainty is rendered irrelevant with our use of strict error tolerances. Note that the significant effects the sign of κ_Δ has on our results would be totally lost with the added approximations invoked by earlier studies [10,19,21,22].

In conclusion, we have demonstrated a versatile state-of-the-art theoretical treatment of electric-field effects in block-copolymer thin films. For our example of a parallel lamellar layer, a peristaltic mode produces the desired reorientation of domains, and is favored by a thin central domain composed of the low-dielectric material. With its impeccable track-record [1], SCFT will undoubtedly provide equally reliable predictions for related issues, such as multilamellar modes [13], defects [18], mobile ions [21], and added solvent or homopolymer [22].

We thank T. P. Russell for useful discussions.

Note added.—Recently, a similar SCFT-based treatment [23] was published.

[1] F. S. Bates and G. H. Fredrickson, Phys. Today **52** No. 2, 32 (1999).
[2] I. W. Hamley, Nanotechnology **14**, R39 (2003).
[3] S. A. Jenekha and X. L. Chen, Science **283**, 372 (1999); A. S. Zalusky *et al.*, J. Am. Chem. Soc. **124**, 12 761 (2002).
[4] D. Zhao *et al.*, Science **279**, 548 (1998).
[5] M. Templin *et al.*, Science **278**, 1795 (1997); W. A. Lopes and H. M. Jaeger, Nature (London) **414**, 735 (2001).
[6] M. Park *et al.*, Science **276**, 1401 (1997).
[7] J. T. Chen *et al.*, Macromolecules **28**, 5811 (1995).
[8] T. Thurn-Albrecht *et al.*, Science **290**, 2126 (2000).
[9] P. Mansky *et al.*, Science **275**, 1458 (1997); J. Genzer and E. J. Kramer, Phys. Rev. Lett. **78**, 4946 (1997); E. Haung *et al.*, Nature (London) **395**, 757 (1998).
[10] K. Admundson *et al.*, Macromolecules **26**, 2698 (1993); **27**, 6559 (1994).
[11] T. L. Morkved *et al.*, Science **273**, 931 (1996).
[12] M. W. Matsen, J. Phys. Condens. Matter **14**, R21 (2002).
[13] A. Onuki and J. Fukuda, Macromolecules **28**, 8788 (1995).
[14] Y. Tsori and D. Andelman, Macromolecules **35**, 5161 (2002).
[15] M. W. Matsen, Phys. Rev. Lett. **80**, 4470 (1998).
[16] M. Laradji *et al.*, Phys. Rev. Lett. **78**, 2577 (1997).
[17] M. W. Matsen, J. Chem. Phys. **106**, 7781 (1997).
[18] T. Xu, C. J. Hawker, and T. P. Russell, Macromolecules **36**, 6178 (2003).
[19] T. Xu *et al.*, Macromolecules **37**, 6980 (2004).
[20] M. Sferrazza *et al.*, Phys. Rev. Lett. **78**, 3693 (1997).
[21] Y. Tsori *et al.*, Phys. Rev. Lett. **90**, 145504 (2003).
[22] A. Böker *et al.*, Macromolecules **36**, 8078 (2003).
[23] C.-Y. Lin, M. Schick, and D. Andelman, Macromolecules **38**, 5766 (2005).